Experiments in Fluids 8, 33–40 (1989)

Experiments in Fluids

Rotation effects on a fully-developed turbulent pipe flow

M. Anwer and **R. M. C. So**

Mechanical and Aerospace Engineering, Arizona State University, Tempe, AZ 85287-6106, USA

Abstract. A fully-developed turbulent pipe flow is allowed to pass through a rotating pipe section, whose axis of rotation coincides with the pipe axis. At the exit end of the rotating section, the flow passes into a stationary pipe. As a result of the relaxation of surface rotation, the turbulent flow near the pipe wall is affected by extra turbulence production created by the large circumferential shear strain set up by the rapid decrease of the rotational velocity to zero at the wall. However, the flow in the most part of the pipe is absent of this extra turbulence production because the circumferential strain is zero as a result of the solid-body rotation imparted to the flow by the rotating pipe section. The combined effect of these two phenomena on the flow is investigated in detail using hot-wire anemometry techniques. Both mean and turbulence fields are measured, together with the wall shear and the turbulent burst behavior at the wall. A number of experiments at different rotational speeds are carried out. Therefore, the effects of rotation on the behavior of wall shear, turbulent burst at the wall, turbulence production and the near-wall flow can be documented and analysed in detail.

List of symbols

a	radius of the pipe
C_{f1}	friction coefficient, $\tau_w/\frac{1}{2}\varrho\, W_0^2$
C_{f2}	friction coefficient, $\tau_w/[\frac{1}{2}\varrho\,(W_0^2+(a\Omega)^2)]$
D	diameter of the pipe
$E_{\tau_w}(f)$	energy spectrum of shear stress
f_b	dimensional burst frequency
$\bar{f}_b$	normalized burst frequency, $\dfrac{f_b}{(f_b)_0}$
F	normalized kurtosis, $\dfrac{(\overline{\tau_w'^4})/(\overline{\tau_w'^2})^2}{[(\overline{\tau_w'^4})/(\overline{\tau_w'^2})^2]_0}$
k	threshold level (used in VITA)
N_s	swirl number, $a\Omega/W_0$
$P(T)$	probability of inter-burst time, T
r	radial coordinate
S	normalized skewness, $\dfrac{(\overline{\tau_w'^3})/(\overline{\tau_w'^2})^{3/2}}{[(\overline{\tau_w'^3})/(\overline{\tau_w'^2})^{3/2}]_0}$
t	integration time (used in VITA)
T_B	mean inter-burst time, $1/f_b$
$\bar{T}_B$	normalized scaled burst frequency, $\dfrac{w_\tau^2\, T_B/\nu}{(w_\tau^2\, T_B/\nu)_0}$
U, V, W	mean velocity components in radial, circumferential and axial directions, respectively
u', v', w'	fluctuating components of velocity in radial, circumferential and axial directions, respectively
W_0	axial bulk mean velocity
w_τ	friction velocity, $\left(\dfrac{\tau_w}{\varrho}\right)^{1/2}$
X	distance measured from the entrance of the bend
δ	thickness of the viscous layer
ν	kinematic viscosity
ϱ	density of fluid
σ	normalized standard deviation, $\dfrac{(\overline{\tau_w'^2})^{1/2}}{(\overline{\tau_w'^2})_0^{1/2}}$
Ω	rotational speed of pipe in RPM

Subscript

0	condition at $X/D=-18$

1 Introduction

When a turbulent wall shear flow is subjected to axial rotation, a destabilizing and/or a stabilizing effect would result depending on the flow condition. Here, the term destabilizing is used to describe the phenomenon of extra turbulence production created by flow rotation, while the term stabilizing is used to describe the rotating flow characteristics without the extra turbulence production present. In the case of a flow through an axially rotating pipe with uniform entrance velocity, flow regions with extra turbulence production present (destabilizing) or absent (stabilizing) could be found in different parts of the pipe. Near the entrance, the wall boundary layer is very thin. Therefore, fluid rotation has to decrease quickly from pipe rotation at the wall to zero outside of the wall boundary layer. The flow near the wall is subjected to a very high mean circumferential shear strain and turbulence production is greatly enhanced. As a result, the near-wall flow is destabilized by rotation. Far downstream, the flow becomes fully-developed and the fluid rotates as a solid body. Since the solid-body rotation curve has a constant slope, turbulence production due to the mean circumferential shear strain is zero. Consequently, rotation gives rise to a stabilizing effect on the flow. In the region spanning the entrance and the fully-developed region, the flow is subjected to both destabilizing and stabilizing effects

of rotation. However, the transition from destabilizing to mixed to stabilizing effect occurs over a finite region and depends on many factors; among these are inlet flow condition and pipe Reynolds number. This three-dimensional flow has been investigated by Murakami and Kikuyama (1980) and Kikuyama et al. (1983).

For external boundary-layer flows with rotation, such as one represented by the flow along an axially rotating cylinder (Bissonnette and Mellor 1974; Lohmann 1976), only a destabilizing effect is present in the boundary layer. This is a consequence of the presence of a large mean circumferential shear strain, created by cylinder rotation, in the boundary layer. As a result, turbulence production is greatly enhanced across the boundary layer (Bissonnette and Mellor 1974). The effect due to cylinder rotation is always destabilizing because, no matter how long is the cylinder, fluid rotation inside the boundary layer will not asymptote towards a solid body. In this flow, there is also no mixed region where stabilizing and destabilizing effects are of equal importance. Therefore, it is not an appropriate flow to investigate if the combined stabilizing and destabilizing effects are to be examined.

In the cases of rotating pipe flows and boundary-layer flows along rotating cylinders, the plane of rotation and the plane of the mean shear do not coincide. As a result, all three turbulent shear stresses are non-zero. When the plane of rotation and the plane of the mean shear coincide, two of the turbulent shear stresses vanish and the complexity of the flow is greatly reduced. Such a flow can be found in a two-dimensional channel rotating about an axis normal to the flow direction. When the flow in the channel is fully developed, a stabilizing effect prevails near one side of the channel while a destabilizing effect dominates the flow on the opposite side of the channel (Johnston et al. 1972). The stabilizing and destabilizing effect switches sides when the rotation is reversed. Johnston et al. (1972) found that the rate of sub-layer bursting was reduced by the stabilizing effect and enhanced by the destabilizing effect. In addition, large-scale roll cells were observed on the destabilized side of the channel. However, they did not report any turbulence measurements. Consequently, the characteristics of combined stabilizing and destabilizing effects on a fully-developed turbulent flow are not known.

The present experiment is designed to study the combined stabilizing and destabilizing effects of rotation on fully-developed turbulent flows. Instead of examining the developing flow in a rotating pipe (Kikuyama et al. 1983) or investigating the flow in a rotating channel whose axis of rotation is normal to the flow direction (Johnston et al. 1972), the present approach chooses to investigate the effect of a sudden relaxation of pipe rotation on a fully-developed turbulent pipe flow. The fully-developed turbulent pipe flow is allowed to pass from a stationary pipe, through a rotating section, and then exit into another stationary section of the pipe again. The flow is forced to achieve a solid-body like rotation within the rotating section. Upon leaving the rotating section, the flow very near the wall is immediately subjected to the action of a large mean circumferential shear strain due to the sudden relaxation of surface rotation. Therefore, the flow downstream of the rotating section is influenced by both stabilizing and destabilizing effects.

2 Experimental set-up and measurement techniques

The experiments are carried out in the curved pipe rig of Anwer and So (1988), which consists of two straight pipes, 7.62 cm in diameter and ~ 100 diameters in length, connected by a 180° bend. A rotating section, six diameters long, is installed in the upstream straight pipe. The rotating section has an I.D. slightly larger than the O.D. of the straight pipe and is supported by roller bearings mounted at each end. A 2.5 HP variable-speed motor is used to rotate the section via a belt drive. The rotating section is located at 6 diameters upstream of the curved bend (Fig. 1). The interior of the section is filled with honeycomb sections, each 5 cm long. The honeycomb sections have a 6 mm cell size and are separated by 24×24 wire mesh screens. This arrangement helps to create a solid-body rotation on the flow exiting from the rotating section. According to Anwer and So (1988, 1989), the turbulent pipe flow at 18 diameters upstream of the curved bend is fully-developed and the normalized characteristics at a pipe Reynolds number of 50,000 are in good agreement with Laufer's (1954) measurements. Furthermore, the effects of bend curvature are limited to one diameter upstream. Therefore, at four diameters upstream of the curved bend entrance, the flow is not affected by bend curvature at all. Furthermore, at two diameters (or 144 mesh width) downstream of the last wire mesh in the rotating section, the turbulence generated by the honeycomb sections and wire meshes would have decayed to less than 1% of the stream velocity (Loehrke and Nagib 1976; Lumley 1964; Corrsin 1963). Consequently, all measurements are carried out at this location, or two diameters downstream of the rotating section.

A straight and a slanted miniature hot-wire are used to measure the flow at $X/D = -18$ and -4 (Fig. 1). If the flow is measured at different angles of attack to the hot-wires, all components of the mean flow and the Reynolds stress can be resolved (Anwer and So 1989). Furthermore, the total wall shear stress at $X/D = -18$ and -4 is measured using a hot-film type flush-mounted shear stress gauge. The gauge is

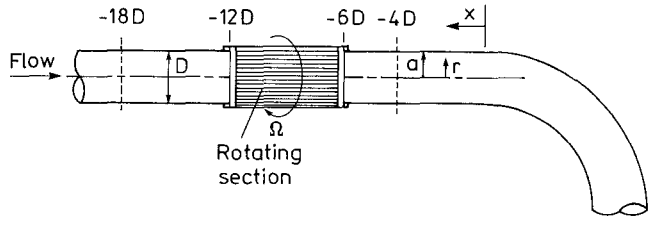

Fig. 1. Schematic of test section

mounted on an aluminum ring which is installed at the measuring locations in such a way that the ring can be rotated around the pipe without leakage present in the joints (Fig. 2). Therefore, the total wall shear around the pipe circumference can be measured easily (Anwer and So 1988). Details of the hot-wire and wall shear measurement techniques are given by Anwer and So (1988, 1989). Further details of the hot-film type shear stress gauge can be found in Menedez and Ramaprian (1985) and Mautner and Van Atta (1986) who used the technique to study unsteady turbulent boundary layers and the characteristics of a turbulent spot, respectively.

A DISA 56C01 constant temperature anemometer, a DISA 56C16 general purpose bridge and a DISA 55N21 linearizer are used to interpret the signals from the sensors. The sensors used are: DISA 55P11 miniature straight-wire probe (sensing element 1.25 mm long and 5 μm in diameter), DISA 55P12 miniature slanted-wire probe (same size as 55P11) with the sensing element mounted at 45° to the probe axis, and a DISA 55R45 flush-mounted hot-film probe. Both the straight and slanted wires are calibrated in a free air jet and the calibration curves are found to be quite repeatable.

The hot-film probe is 0.2 mm wide and 0.75 mm in length. Therefore, the sensing element corresponds to 15 viscous lengths, which is well within the limit proposed by Ligrani and Bradshaw (1987) for accurate measurements of the properties of the small-scale turbulence in the near-wall region. Furthermore, heat transfer from a sensor placed in the substrate (like the hot-film probe used in this study) is different from the heat transfer from a probe placed in the flow. Consequently, the frequency response of a wall-mounted probe may be of crucial concern (Bellhouse and Schultz 1966). The frequency response of the wall-mounted sensor used in this study is estimated to be of the order of 100 kHz (Bellhouse and Schultz 1966). This is almost two orders of magnitude larger than the dynamic range of the flow estimated from the Kolmogorov time scale. The hot-film type shear stress gauge is calibrated in the present test rig with a fully-developed turbulent flow established at the measurement location. Again, the calibration curve shows little or no shift with time.

All the signals are digitized using a Metrabyte DAS-16, 12 bit resolution A/D converter. Sampling rate for the hot-wire signals is selected to be 3 KHz and a record length of 10 s is used to calculate the flow characteristics. On the other hand, a sampling rate of 20 KHz is chosen for the wall shear stress signal. This high sampling rate is necessary because the bursting event itself is very short. Therefore, it is necessary to collect as many data points as possible in this short interval. Three data records of 1 s each are collected for analysis. Finally, a stroboscope accurate to 1 RPM is used to measure the rotational speed of the rotating section.

Altogether 11 sets of experiments at different Ω (RPM) are carried out. The total wall shear is measured together with the flow characteristics. However, detailed measurements of the flow properties are carried out only at $N_s = 0.0$, 0.5 and 1.0. In addition, the flow properties at $X/D = -18$ are also measured, so that the disturbances, created by the rotating section, on the fully-developed pipe flow can be properly documented and accounted for in the assessment of rotation effects. All the experiments are carried out at $W_0 \approx 10$ m/s, corresponding to a pipe Reynolds number of 50,000.

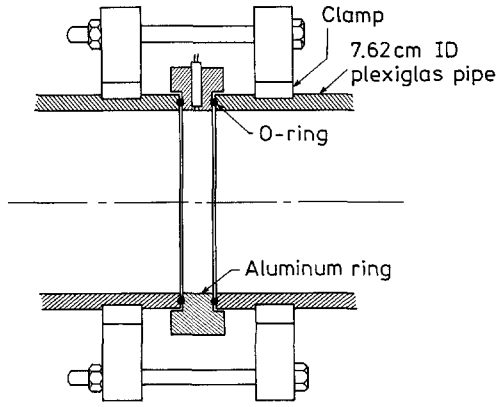

Set-up for shear-stress measurement

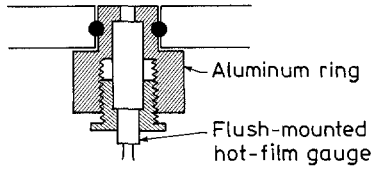

Close-up of shear stress gauge

Fig. 2. Details of wall shear measurement

Besides the total wall shear stress, the shear stress signals are also analyzed for turbulent burst behavior at the wall. The Variable Interval Time Averaging (VITA) technique is used to detect bursts in the wall shear stress signal. Details of this technique are provided by Blackwelder and Kaplan (1976) and Chen and Blackwelder (1978). Since the VITA technique is essentially a mathematical low pass filter, turbulent burst detection is a strong function of the integration time t and the threshold level k. The effects of t and k on the number of bursts detected have been examined by Johansson and Alfredsson (1982). Blackwelder and Kaplan (1976) propose a value for $k = 1.2$ and a non-dimensional integration time of $t w_\tau^2/\nu = 10$. For the present analysis, $k = 1.2$ and $t w_\tau^2/\nu = 17$ are chosen. According to Anwer and So (1988), these values of t and k give a burst frequency for a fully-developed pipe flow that is consistent with other measurements (Sabot and Comte-Bellot 1976; Achia and Thompson 1977). The choice of these values is not too critical for the present study because the absolute burst frequency is not important. Rather, the relative increase of the burst frequency under the influence of rotation is more significant. Therefore, once the threshold value and the integra-

tion time have been decided upon, the same values are used throughout the study so that the relative effects of rotation on the burst frequency can be properly assessed.

3 Discussion of results

A cylindrical coordinate system is used to describe the flow of the present experiments with X denoting the axial direction and measures zero at the entrance to the curved bend and r representing the radial direction. In this flow, the plane of rotation and the plane of the mean shear do not coincide. Therefore, $\overline{v'w'}$ and $\overline{u'v'}$ are not necessarily zero. The hot-wire technique used measures all three components of the mean flow and all six components of the Reynolds stress. These, together with the wall shear data, are discussed under the following headings: (1) mean and turbulence field behavior, (2) wall shear variation and (3) turbulent burst behavior. The values of the various quantities used to normalize the flow properties are summarized here as: $(C_{f1})_0 = (C_{f2})_0 = 2.3 \times 10^{-3}$, $(f_b)_0 = 46$ events/s, $(w_\tau^2\, T_B/\nu)_0 = 153.2$, $(\overline{\tau_w'^2})_0^{1/2} = 4.8 \times 10^{-3}$ (N/m^2), $[(\overline{\tau_w'^3})/(\overline{\tau_w'^2})^{3/2}]_0 = 0.348$ and $[(\overline{\tau_w'^4})/(\overline{\tau_w'^2})^2]_0 = 2.78$.

3.1 Mean and turbulence field behavior

The results for the three different N_s cases are shown in Figs. 3–6. In these figures, the measurements obtained at $X/D = -18$, or six diameters upstream of the rotating section, are also plotted for comparison. As expected, the flow is axisymmetric and the mean radial velocity, U, is zero everywhere. Therefore, only the U distribution for the $N_s = 0$ case is shown in Fig. 3. The V velocity is also zero everywhere for the $N_s = 0$ case. Thus, the scatter shown in Fig. 3 serves to illustrate the accuracy of the present measurements. For the $N_s > 0$ cases, the distribution of V is indeed given by a solid-body rotation curve. The linear behavior extends all the way to the measurement point closest to the wall, which is at $r/a = 0.94$. This gives an approximate estimate of the thickness of the viscous layer, δ, which is at most given by 0.06a. The axial velocity distributions at $X/D = -18$ and -4 for the $N_s = 0$ case is essentially identical. Therefore, little or no disturbance to the flow is created by the passage of the fully-developed pipe flow through the rotating section, and the flow inside the rotating section can again be considered as fully-developed turbulent pipe flow. The effect of rotation is to flatten the W profile, thus creating a more uniform W distribution across the pipe (Fig. 3).

Since V/r is constant over 90% of the pipe diameter, turbulence production by the mean circumferential shear strain, $r\partial(V/r)/\partial r$, is zero over this portion of the pipe. However, the turbulent normal stresses in the region away from the pipe wall are greatly enhanced by rotation (Fig. 4). The increase cannot be attributed to disturbances brought on by the rotating section, because the measured distribution of $(\overline{w'^2})^{1/2}$ at $X/D = -18$ is practically the same as that obtained at $X/D = -4$ for the $N_s = 0$ case. Furthermore, the studies of Corrsin (1963), Lumley (1964) and Loehrke and Nagib (1976) show that, at $X/D = -4$, the turbulence generated by the honeycomb sections and wire meshes would have decayed to less than 1% of W_0 and can hardly account for the differences shown in $(\overline{w'^2})^{1/2}$ for the three cases: $N_s = 0$, 0.5 and 1.0 (Fig. 4). The enhancement of all the normal stresses increases with N_s and, at $N_s = 1$, the distributions of $(\overline{v'^2})^{1/2}$ and $(\overline{u'^2})^{1/2}$ across the pipe are close to uniform. This increase in normal stresses has to come from turbulence production very near the wall, where $r\partial(V/r)/\partial r$ is not zero. Once produced, the turbulence energy is immediately transported away from the wall and into the pipe core. This energy transport contributes to the flattening of the W profile as N_s increases.

The shear stress $\overline{u'v'}$ is identically zero across the pipe. So is $\overline{v'w'}$, except in a region very close to the wall, where $V/a\,\Omega$ decreases from one to zero at the wall (Fig. 5). If the location where $\overline{v'w'}$ starts to deviate from zero is taken to be a measure of δ, then δ is again determined to be $\sim 0.06a$. This can be taken to indicate that turbulence production due to rotation is limited to within the viscous wall layer of thickness δ. On the other hand, $\overline{w'u'}$ starts to deviate from the linear distribution as early as $r/a = \pm 0.5$. Most likely, this is the result of turbulence production by the mean strain $\partial W/\partial r$. Within the viscous wall layer, the shear stress $\overline{v'w'}$ is quite a bit larger than $\overline{w'u'}$ and becomes the dominant shear stress in the flow. The total shear stress, given by $[(\overline{w'u'})^2 + (\overline{v'w'})^2]^{1/2}$, is plotted in Fig. 6. In the same plot is also shown the wall shear measurements obtained from the hot-film type shear stress gauge. The hot-wire measurements asymptote correctly to the wall shear values, which are essentially the same on opposite sides of the pipe and reaffirms the axial symmetry of the flow. However, the measurement next to the wall is consistently too high. Possible errors are wall effect on hot-wire measurement, finite wire length, velocity gradient effect, etc. Overall, the measurements are very consistent and show that rotation increases wall shear substantially. Most of that increase comes from $vr\partial(V/r)/\partial r$. Furthermore, the hot-wire measurements substantiate the fact that the wall shear stress gauge measures the total wall shear rather than the wall shear along the axial flow direction only.

3.2 Wall shear variation

The variations of wall shear around the pipe at $X/D = -18$ and -4 have been measured for the $N_s = 0$, 0.5 and 1.0 cases. At $X/D = -18$, the circumferential variations of the wall shear stress are found to be no more than $\pm 2\%$ and the measurements are essentially identical to those reported by Anwer and So (1988). Uniform wall shear is also obtained at $X/D = -4$ for the three cases studied. Again, the variations are similar to those measured at $X/D = -18$. Consequently, the axisymmetric nature of the flow is confirmed. The variation of wall shear with N_s is shown in Fig. 7. Here, the skin

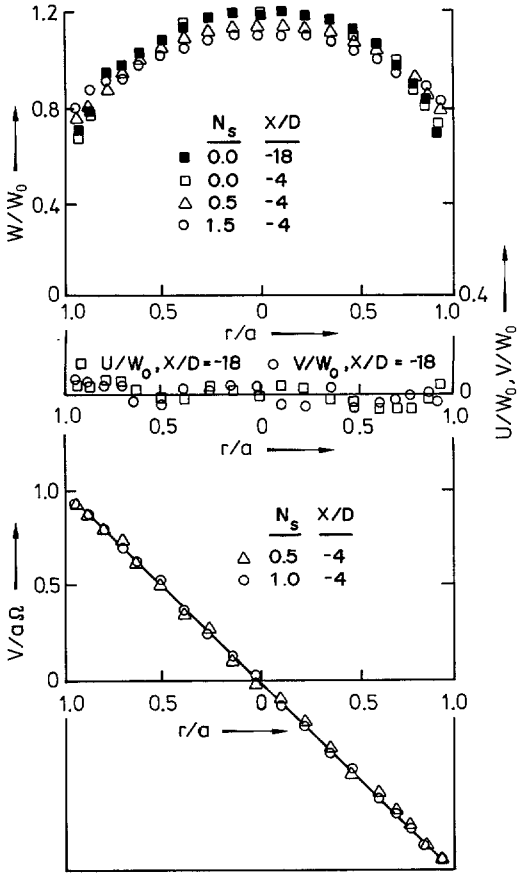

Fig. 3. Variation of mean flow behavior with N_s

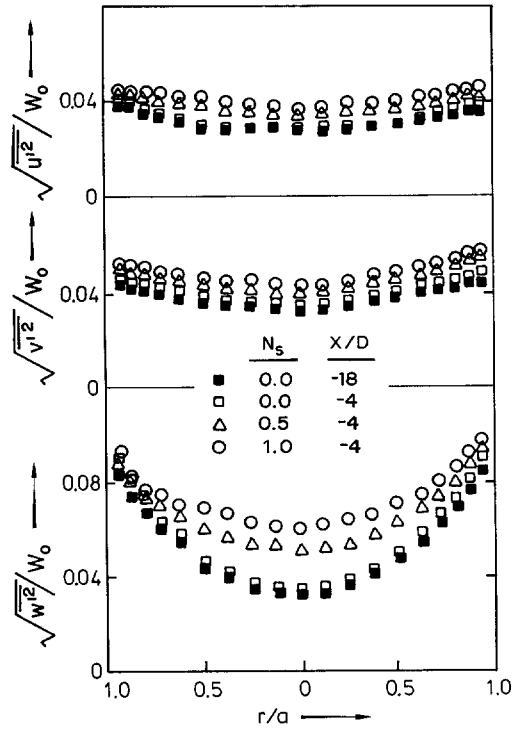

Fig. 4. Variation of normal stress behavior with N_s

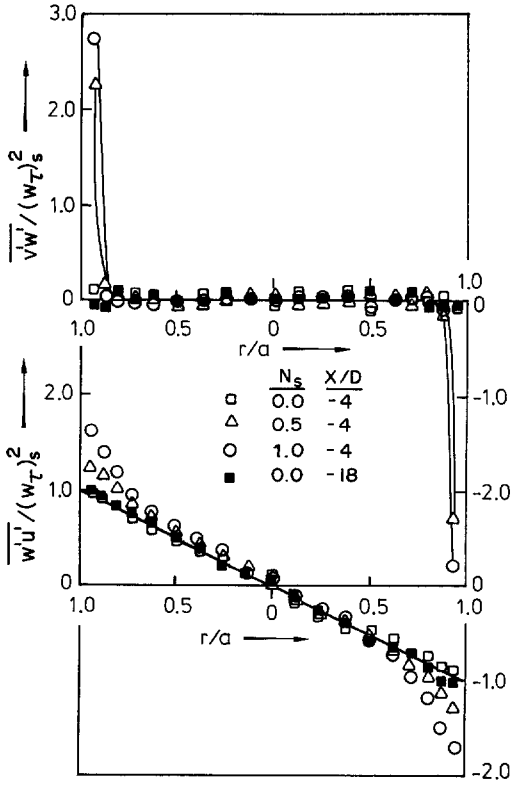

Fig. 5. Variation of shear stress behavior with N_s

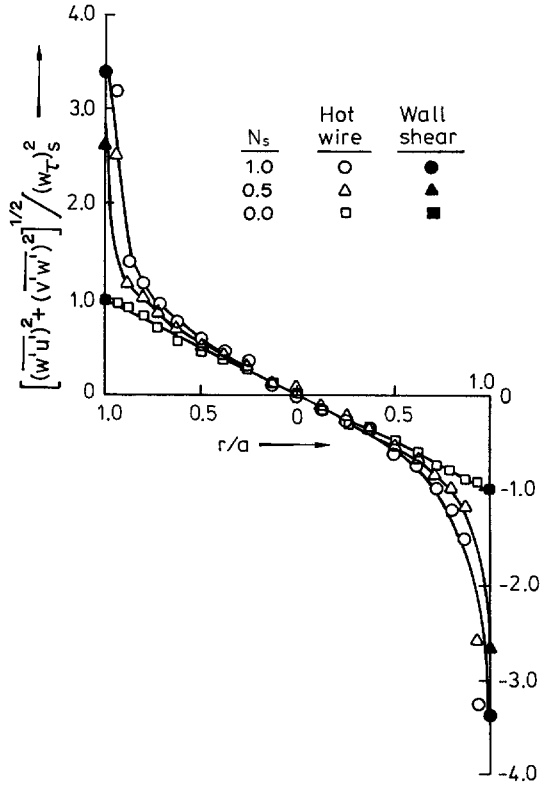

Fig. 6. Total shear stress behavior variation with N_s

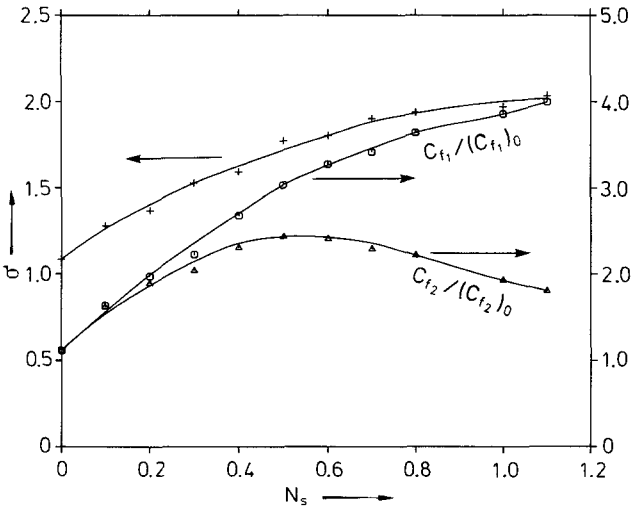

Fig. 7. Variations of skin friction coefficients and σ with N_s

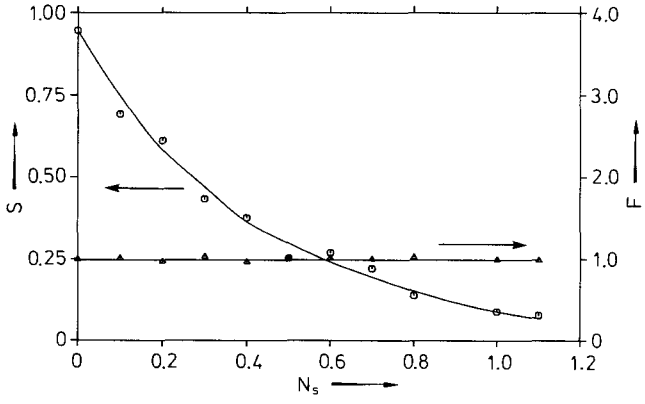

Fig. 8. Variations of S and F with N_s

friction coefficients, C_{f1} and C_{f2}, are plotted together with the normalized rms value of wall shear, σ. In order to discern the true behavior of the skin friction coefficient, two coefficients are defined; one normalized by $\frac{1}{2}\varrho W_0^2$ while another is normalized by $\frac{1}{2}\varrho(W_0^2 + a^2\Omega^2)$. The relative increase in C_{f1} and C_{f2} is shown in Fig. 7 by normalizing these quantities by the respective values at $X/D = -18$. Even though the rotating section does not appreciably disturb the turbulent pipe flow, it does impart more frictional loss to the flow. As a result, the skin friction coefficient at $X/D = -4$ is about 13% higher than its value at $X/D = -18$; the increase in the skin friction coefficient due to rotation is substantial. At $N_s = 1$, C_{f1} is about 3.8 times its value at $N_s = 0$. Most of this increase comes from the contribution $vr\partial(V/r)/\partial r$. The increase in C_{f1} is essentially linear in the region $0 < N_s < 0.4$ and tapers off gradually in the region $N_s > 0.4$. This definition of skin friction coefficient is not very physical because the trend tends to indicate a finite C_{f1} as Ω increases to a very large value. On the other hand, the plot of C_{f2} indicates that the skin friction coefficient increases with N_s to a maximum at $N_s = 0.5$ and then decreases with N_s beyond $N_s = 0.5$. This trend implies that as Ω becomes larger and larger, C_{f2} would eventually become very small, which is more consistent with our physical expectation. The maximum C_{f2} reached at $N_s = 0.5$ is about 2.5 times its value at $X/D = -18$. Therefore, it can be concluded that pipe rotation enhances C_{f2} substantially in the region $0 < N_s < 0.5$. Beyond this region, further increase in Ω causes C_{f2} to decrease.

The behavior of σ with respect to N_s is similar to that of C_{f1}, except that σ increases by a factor of 2 only. On the other hand, the normalized skewness, S, shows a steady decline from ~ 0.90 at $N_s = 0$ to ~ 0.09 at $N_s = 1$ (Fig. 8). This means that the turbulent flow near the wall is becoming more and more Gaussian as rotation is increased. This result is consistent with the mean W and normal stress results shown in Figs. 3 and 4. The normalized kurtosis, F, is not affected by rotation and its value is approximately one in the range of N_s investigated (Fig. 8).

The measurements examined up to this point clearly show that the flow is axisymmetric and is greatly affected by the destabilizing effect created by the large mean circumferential shear strain near the pipe wall. Turbulence production near the wall is substantially increased. Once produced, the turbulence energy is immediately transported away from the wall and into the pipe core. The normal stresses in the most part of the pipe core increase as a result and become more uniform across the pipe. All these processes are taking place in spite of the existence of a stabilizing effect over 90% of the pipe diameter due to rotation.

3.3 Turbulent burst behavior

The burst frequency is determined from the wall shear signal using the VITA technique. Three records of 1 s each are collected, therefore, the result shown represents the ensemble average of the three records. Since the relative effects of rotation on the burst phenomenon are of interest only, the conventional way of presenting f_b by normalizing it with outer variables (a and W_0) and/or inner variables (ν and w_τ) is not adopted here. Instead, the values of $\bar{f}_b$ and $\bar{T}_B$ are plotted versus N_s in Fig. 9. Here, the burst frequency and mean inter-burst time are normalized by their values at $X/D = -18$. Therefore, the plot shows the relative effects of rotation on $\bar{f}_b$ and $\bar{T}_b$. It can be seen that $\bar{f}_b$ increases as N_s increases. The initial increase in the region $0 < N_s < 0.4$ is slow. However, at $N_s \geq 0.4$, the increase in $\bar{f}_b$ with N_s is approximately linear. This shows that high circumferential shear promotes turbulent bursts at the wall, a phenomenon not unlike that found by Anwer and So (1988) in the flow along the top of a curved bend. In the curved flow case, the increase is small, $\sim 20\%$, because the secondary velocity is small compared to the axial flow velocity. For the present experiment, the increase amounts to over 50% at $N_s = 1$. These results show that, as long as there is a circumferential velocity in the near wall region, turbulent bursts at the wall is enhanced. It does not matter whether this circumferential

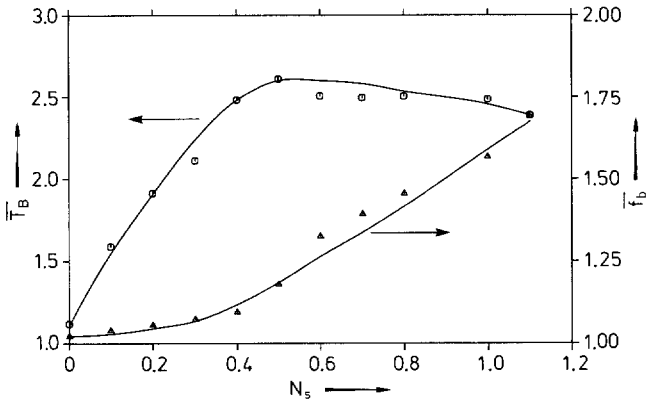

Fig. 9. Burst frequency variation with N_s

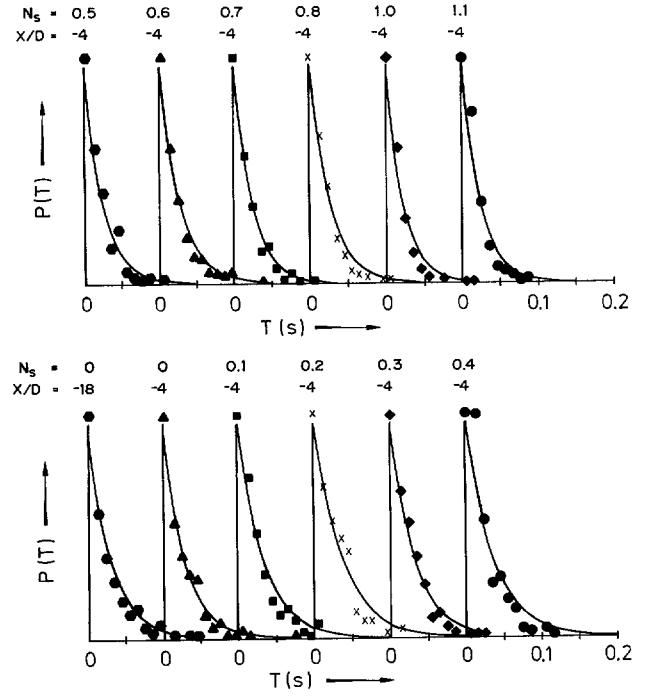

Fig. 10. Distributions of inter-burst time

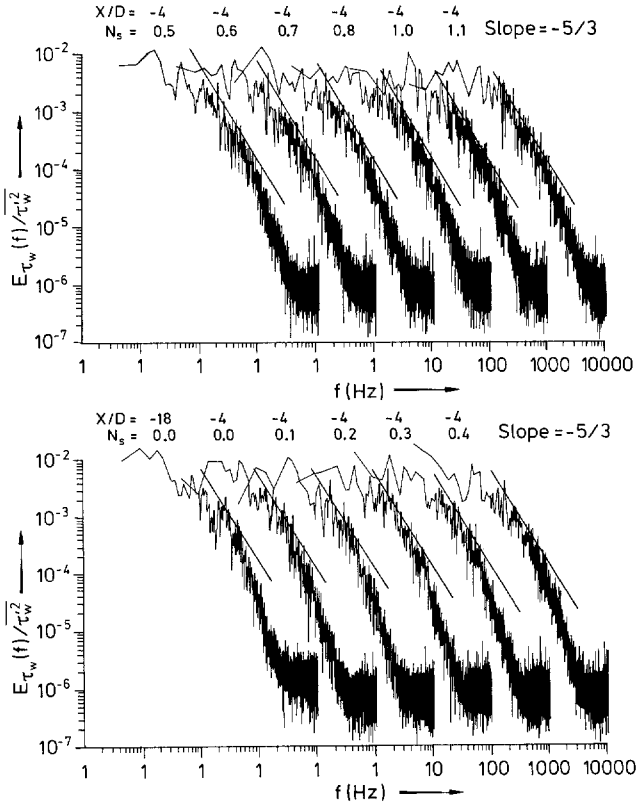

Fig. 11. Spectral distributions of wall shear

velocity is created by pipe rotation or by bend curvature. On the other hand, the plot of $\overline{T}_B$ versus N_s shows that $\overline{T}_B$ increases to a maximum and then starts to slowly decrease beyond $N_s \approx 0.5$ (Fig. 9). The increase in $\overline{T}_B$ is about 260% above its value at $X/D = -18$, and suggests that the inter-burst time becomes longer as N_s increases to about 0.5.

Recently, several researchers (Shah and Antonia 1987; Luchik and Tiederman 1987; Blackwelder and Haritonidis 1983) have argued that the inner variables are the correct scaling parameters for sub-layer bursting. The present result tends to confirm this argument because the trend of $\overline{T}_B$ is very similar to $C_{f2}/(C_{f2})_0$, while the trend of $\overline{f}_b$ is not (compare Figs. 8 and 9). Therefore, this means that, even for flows under the influence of axial rotation, the proper scalings for f_b are the inner variables and the results show that local flow similarity has been reached at or near $N_s = 0.5$. This behavior is consistent with the variation of $C_{f2}/(C_{f2})_0$ with N_s and suggests that the increase in C_{f2} is associated with an increase in turbulent burst activities.

If the turbulent burst phenomenon at the wall is random in both time and space, then the inter-burst time should have an exponential distribution. Bogard and Tiederman (1986, 1987) show that the inter-burst time in a turbulent channel flow indeed has an exponential distribution. Previous results on the wall shear and the turbulence field tend to indicate that the flow is becoming more random and isotropic. If this is true, then a plot of the inter-burst time would show that the measurements are better correlated by an exponential distribution as N_s increases. Inter-burst time is also calculated in the present analysis and the results are shown in Fig. 10. In addition, a least square exponential fit is calculated using all the actual data points and the results plotted as solid curves in Fig. 10. It can be seen that, as N_s increases the exponential distribution fits the data better and better. Therefore, the wall shear signal is becoming more Gaussian as N_s increases; a conclusion consistent with that drawn above based on other turbulence data.

The energy spectrum of the wall shear stress versus the frequency, f, at different N_s is shown in Fig. 11. Consistent

with other results discussed before, the spectra at $X/D = -18$ and -4 for the case $N_s = 0$ are essentially identical. This further confirms the conclusion that the rotating section does not appreciably perturb the fully-developed turbulent pipe flow except to impart a slightly higher frictional loss to the flow. Consequently, the present study truly represents an investigation of the effects of pipe rotation on a fully-developed turbulent pipe flow. As N_s increases, the equilibrium range of the spectrum, which is characterized by a slope of $-5/3$, is observed to increase. This implies that the wall shear signal is becoming more Gaussian, and is essentially a consequence of the large mean circumferential shear strain's interaction with the turbulence field in the wall layer. Again, this result confirms the above findings based on turbulence measurements and the burst data.

4 Conclusions

An experimental study of the effects of axial rotation on the characteristics of a fully-developed turbulent pipe flow has been carried out. The results show that the relaxation of pipe rotation gives rise to a large mean circumferential shear strain in the viscous wall layer, which, in turn, produces a very significant destabilizing effect on the flow. Even though a stabilizing effect is present over 90% of the pipe diameter because of the solid-body rotation of the fluid, the destabilizing effect completely dominates over the stabilizing effect and enhances the turbulence over the whole pipe. The turbulent normal stresses are observed to increase significantly in the pipe core and to become more uniform across the pipe. The skin friction coefficient C_{f2} increases as N_s is increased. A maximum is reached at $N_s \simeq 0.5$. Thereafter, further increase in N_s leads to a slow decrease of C_{f2} which suggests that, as N_s becomes very large, C_{f2} will eventually become very small. The augmentation of C_{f2} comes mainly from the contribution, $vr\partial(V/r)/\partial r$, and little from the term $v\partial W/\partial r$. Concommitant with the increase in C_{f2} is a significant increase in the burst frequency at the wall. A proper scaling of this burst frequency by inner variables reveals that the non-dimensional frequency essentially follows the same trend as C_{f2}, with a maximum at $N_s \simeq 0.5$ and slow decrease thereafter. This implies that some kind of local flow similarity has been reached at or near $N_s \simeq 0.5$ and that increased shear at the wall is associated with increased turbulent burst activities. Further evidence in support of this interpretation is provided by a detailed analysis of the wall shear stress signals. Finally, the increase in burst frequency bears striking resemblance to that found near the top of a curved bend.

Acknowledgement

Research support from the Office of Naval Research under Grant No. N0014-81-K-0428 is gratefully acknowledged.

References

Achia, B. U.; Thompson, P. W. 1977: Structure of the turbulent boundary layer in a drag reducing pipe flow. J. Fluid Mech. 81, 439–464

Anwer, M.; So, R. M. C. 1988: Study of sublayer bursting in a curved bend. AIAA Paper 88–3581

Anwer, M.; So, R. M. C.; Lai, Y. G. 1989: Perturbation by and recovery from bend curvature of a fully-developed turbulent pipe flow. Phys. Fluids, in press

Bellhouse, B. J.; Schultz, P. L. 1966: Determination of mean and dynamic skin friction, separation and transition in low-speed flow with a thin-film heated element. J. Fluid Mech. 24, 379–400

Bissonnette, L. R.; Mellor, G. L. 1974: Experiments on the behavior of an axisymmetric turbulent boundary layer with a sudden circumferential strain. J. Fluid Mech. 63, 369–413

Blackwelder, R. F.; Haritonidis, J. H. 1983: Scaling of bursting frequency in a turbulent layer. J. Fluid Mech. 132, 87–103

Blackwelder, R. F.; Kaplan, R. E. 1976: On the wall structure of the turbulent boundary layer. J. Fluid Mech. 76, 89–112

Bogard, D. G.; Tiederman, W. G. 1986: Burst detection with single point velocity measurements. J. Fluid Mech. 162, 380–413

Bogard, D. G.; Tiederman, W. G. 1987: Characteristics of ejections in turbulent channel flows. J. Fluid Mech. 179, 1–19

Chen, C. P.; Blackwelder, R. F. 1978: The large scale motion in a turbulent boundary layer: a study using temperature contamination. J. Fluid Mech. 89, 1–31

Corrsin, S. 1963: Turbulence: experimental methods. Handb Phys. 8, 524–590

Johansson, A. V.; Alfredsson, P. H. 1982: On the structure of turbulent channel flow. J. Fluid Mech. 122, 295–314

Johnston, J. P.; Halleen, R. M.; Lezius, D. K. 1972: Effects of spanwise rotation on the structure of two-dimensional fully-developed turbulent channel flow. J. Fluid Mech. 56, 533–557

Kikuyama, K.; Murakami, M.; Nishibori, K. 1983: Development of three-dimensional turbulent boundary layers in an axially rotating pipe. J. Fluids Eng. 105, 154–160

Laufer, J. 1954: The structure of turbulence in fully developed pipe flow. NACA Report 1174

Ligrani, P. M.; Bradshaw, P. 1987: Spatial resolution and measurement of turbulence in the viscous sublayer using subminiature hot-wire probes. Exp. Fluids 5, 407–417

Loehrke, R. I.; Nagib, H. M. 1976: Control of free stream turbulence by means of honeycomb. A balance between suppression and generation. J. Fluids Eng. 98, 342–353

Lohmann, R. P. 1976: The response of a developed turbulent boundary layer to local transverse surface motion. J. Fluids Eng. 98, 354–363

Luchick, T. S.; Tiederman, W. G. 1987: Timescale and structure of ejections and bursts in turbulent channel flows. J. Fluid Mech. 174, 529–552

Lumley, J L. 1964: Passage of a turbulent stream through honeycomb of large length-to-diameter ratio. J. Basic Eng. 86, 218–220

Mautner, T. S.; Van Atta, C. W. 1986: Wall shear stress measurements in the plane of symmetry of a turbulent spot. Exp. Fluids 4, 153–162

Menendez, A. N.; Ramaprian, B. R. 1985: The use of flush-mounted hot film gauges to measure skin friction in unsteady boundary layers. J. Fluid Mech. 161, 139–160

Murakami, M.; Kikuyama, K. 1980: Turbulent flow in axially rotating pipes. J. Fluid Eng. 102, 97–103

Sabot, J.; Comte-Bellot, G. 1976: Intermittency of coherent structures in the core region of fully developed turbulent pipe flow. J. Fluid Mech. 74, 767–796

Shah, D. A.; Antonia, R. A. 1987: Scaling of wall shear stress fluctuations in a turbulent duct flow. AIAA J. 25, 22–29

Received April 4, 1989